

Coherent transport structures in magnetized plasmas *II* :

Numerical results

G. Di Giannatale,¹ M.V. Falessi,² D. Grasso,³ F. Pegoraro,⁴ and T.J. Schep⁵

¹*IGI - CNR Corso Stati Uniti 4, Padova, Italy*

²*ENEA C.R. Frascati Via Enrico Fermi 45 Frascati,*

Dipartimento di Matematica e Fisica, Roma Tre University, Roma, Italy

³*ISC - CNR and Politecnico di Torino*

Dipartimento Energia C.so Duca degli Abruzzi 24, Torino. Italy

⁴*Dipartimento di Fisica E. Fermi, Pisa University,*

largo Pontecorvo 3, Pisa, Italy

⁵*Fluid Dynamics Laboratory, Dep. Applied of Physics, Eindhoven University of Technology, p.o.box 513, 5600MB Eindhoven, The Netherlands*

In a pair of linked articles (called Article *I* and *II* respectively) we apply the concept of Lagrangian Coherent Structures borrowed from the study of Dynamical Systems to magnetic field configurations in order to separate regions where field lines have different kind of behavior.

In the present article, article *II*, by means of a numerical procedure we investigate the Lagrangian Coherent Structures in the case of a two-dimensional magnetic configuration with two island chains that are generated by magnetic reconnection and evolve nonlinearly in time. The comparison with previous results, obtained by assuming a fixed magnetic field configuration, allows us to explore the dependence of transport barriers on the particle velocity.

I. INTRODUCTION

In recent years the concept of Lagrangian Coherent Structures (LCS) has been introduced by G. Haller, i.e. see Ref.1, in the context of transport processes in complex fluid flows. In an accompanying paper, referred to here as Article *I*, it was shown that such a concept can be usefully applied to the study of particle transport in a magnetized plasma in the limit where the field line dynamics can be taken as a proxy for the particle dynamics. In particular in Article *I* it was shown how to relate a magnetic field configuration, at a fixed physical time, to a Hamiltonian system where the role of “time” (Hamiltonian time) is taken by an appropriately chosen coordinate along the magnetic field lines. In the same article, after a brief summary of the so called “lobe-dynamics” and of the related transport in a nonautonomous one-degree of freedom Hamiltonian system, the definition and properties of the Lagrangian Coherent Structures (LCS) were recalled. In the case of a (Hamiltonian) time periodic configuration, i.e. of a configuration that is geometrically periodic in the direction of the magnetic field as is the case e.g. of a toroidal configuration, the connection with the widely used Poincaré map approach was mentioned. Finally in Article *I* the magnetic configuration that is used in the numerical simulations reported in the present paper was introduced and a generalization to the case where the LCS are defined so as to include the evolution of the magnetic configuration in time was discussed. The chosen magnetic configuration is based on the investigation presented in Refs. 2–4 of the nonlinear evolution of two chains of magnetic islands produced by magnetic reconnection.

In the present paper the concepts introduced in Article *I* are implemented numerically using a MATLAB tool developed by K. Onu and G. Haller, see Ref. 5. First the

LCS are obtained by considering a snapshot at a fixed physical time of the evolving magnetic configuration by exploiting explicitly its periodicity in “Hamiltonian” time (see Eq.(20) of Article *I*). Then the same numerical procedure is used to include the evolution of the magnetic configuration in physical time. This allows us to explore the dependence of transport barriers on particle velocity.

This paper is organized as follows. In Sec.II, after recalling the main features of the magnetic configuration of interest, we introduce the adopted numerical computation scheme and briefly describe the precautions that have been used in its implementation. In Sec.III we take the flux function in the magnetic Hamiltonian at a fixed physical time: we choose $t = 415$, i.e. before the onset of fully developed chaos. The corresponding LCS are then obtained numerically and compared to the structures in the Poincaré map: in fact both methods can be used in this case since the corresponding dynamical system is periodic in Hamiltonian time. In Sec.IV we consider the case of a magnetic field that evolves in physical time, i.e. the case where a charged particle moving in the plasma sees a time varying magnetic field during its motion, and apply the simplified model described in Sec. VIB of Article *I*. In this case the corresponding dynamical system turns out not to be periodic in time and the Poincaré map technique cannot be applied. The LCS are then obtained numerically for different particle streaming velocity along field lines with the aim of finding how do the LCS change with physical time, how they differ from those found at the fixed physical time $t = 415$, and, in addition, whether and how particle with different velocities can cross LCS calculated for a different particle velocity. Finally the conclusions are presented.

II. SIMULATION SETTINGS AND NUMERICAL PROCEDURE

A. Magnetic configuration

As anticipated in Sec. VI of Article *I*, in the present article we study the LCS in a magnetic configuration of the form

$$\mathbf{B}_{eq} = B_0 \mathbf{e}_z + \nabla \psi(x, y, z, t) \times \mathbf{e}_z, \quad (1)$$

where $\psi(x, y, z, t)$ is the full magnetic flux function that includes the equilibrium and the time evolving perturbations. Periodicity is assumed in all three directions and the configuration is restricted to the domain $[-L_x, L_x] \times [-L_y, L_y] \times [-L_z, L_z]$ with $L_x = \pi, L_y = 2\pi, L_z = 16\pi$. We recall that the expression of $\psi(x, y, z, t)$ that we use has been obtained by means of a numerical simulation in Ref.2 (see also Refs.3 and 4) by imposing a ‘‘double helicity’’ perturbation $\hat{\psi}_1(x, t) \cos(k_{1y}y + k_{1z}z) + \hat{\psi}_2(x, t) \cos(k_{2y}y + k_{2z}z)$, with $k_{iy} = m_i\pi/L_y$ and $k_{iz} = n_i\pi/L_z$ where $m_1 = m_2 = 1$ and $n_1 = 1, n_2 = 0$, on an equilibrium of the form $\psi_{eq}(x) \propto \cos(x)$. The field line equations are given by

$$\frac{dx}{dz} = -\frac{\partial\psi}{\partial y}, \quad \frac{dy}{dz} = \frac{\partial\psi}{\partial x}. \quad (2)$$

Perturbations with different ‘‘helicities’’ are required in order to make the Hamiltonian system described in Sec. II of Article *I* non integrable, i.e., to generate a chaotic magnetic configuration. In the following analysis we will focus on the magnetic configuration at two different normalized (respect to the Alfvén time) physical times, i.e. $t = 415$ and $t = 425$, in which chaos, initially developed only on a local scale (at $t = 415$), starts to spread on a global scale (at $t = 425$).

In order to minimize the computational effort, we simplify the Hamiltonian by imposing a threshold condition on the amplitude of the components of the Fourier expansion of $\psi(x, y, z, t)$ along x, y and z . The validity of this approximation has been tested in Ref. 3. The physical time evolution of $\psi(x, y, z, t)$ between $t = 415$ and $t = 425$ was found in Ref. 2 to be super-exponential and is modeled here by interpolating the coefficients of its Fourier expansion according to a quadratic exponential time law of the form

$$\exp \gamma_{k_y, k_z} (t - t_1)^2 \quad \text{for } t > t_1 = 415, \quad (3)$$

where we assume that the coefficients γ_{k_y, k_z} depend only on the mode numbers k_y and k_z .

B. LCS computation scheme

In order to find the hyperbolic Lagrangian Coherent Structures, we use a MATLAB tool developed by K. Onu and G. Haller, see Ref. 5. This tool detects the LCS on

the basis of their characterization as the most repelling or attractive material lines advected within the fluid and relies on the definitions that we listed in Secs. V and VA of Article *I*.

The key steps of the adopted procedure can be summarized by the following operations:

1. Defining a velocity field
2. Computing the eigenvalues and eigenvectors of the Cauchy-Green strain tensor
3. Filtering the data by setting the value of some parameters requested by the numerical tool and aimed at locating the most important LCS to characterize the system dynamics. Detail on this filtering procedure will be given below.
4. Finally detecting the LCS

The procedure starts with the integration of the Hamilton equations, Eq.(2), for the magnetic field lines. This enables us to calculate the flow map $\phi_{z_0}^z(x_0, y_0)$ (defined in Eq.(4) of Article *I*) with z substituted for t and then to compute the Cauchy-Green strain tensor field, its eigenvalues and eigenvectors and the FTLE field. The repelling LCS are then found following the conditions given in Sec. V A of Article *I*. In particular, in lieu of Eq.(14) but following Ref. 5, we identify the strongest repelling curves as those passing through a local maximum of the FTLE field.

The advantage of such a prescription is twofold: on the one hand it significantly reduces the computing time and on the other hand it allows us to avoid the ambiguities related to the implementation of condition (14) of Article *I*, that is $\boldsymbol{\xi}_{max} \cdot \nabla^2 \lambda_{max} \cdot \boldsymbol{\xi}_{max} < 0$, on a discrete relatively sparse grid. Therefore, since we need a point from which to start the numerical integration of LCS, we take the largest local maxima of FTLE field as starting points. In principle, we should solve for the curve defined by the condition $\mathbf{e}_0 = \boldsymbol{\xi}_{min}$ (Eq.(12) of Article *I*) where we recall \mathbf{e}_0 is the tangent vector to the material line and $\boldsymbol{\xi}_{min}$ the eigenvector of the Cauchy-Green strain tensor corresponding to the smaller eigenvalue) starting from each local maximum. However in chaotic systems the FTLE field exhibits a huge number of local maxima and, in addition, the numerical evaluation of the matrix $\nabla \phi_{z_0}^z(x_0, y_0)$ produces a very discontinuous FTLE field. By integrating the above condition for each local maximum we would find so many structures that they would confuse the physical information which we want to extract. For these reasons it is necessary to define a criterion to adopt in order to filter out the maxima that we consider not to be physically significant. It is clear that the larger the area around a local maximum, the more significant the maximum can be assumed to be. This criterion corresponds to take only those points that are absolute maxima of FTLE field within a predefined area. Therefore, we seek maxima of FTLE field and then, if the distance between two maxima is smaller than the predefined maximization distance, we disregard the maximum with the lower value of the FTLE field. In other words the number of LCS that we find depends on the

value that we choose for the maximization distance in the code.

In order to clarify this criterion let us suppose that two large maxima of the FTLE field are very close to each other, i.e. that their distance is smaller than the chosen maximization distance. In this case only the largest maximum is used as a starting integration point. In general this does not lead to a loss of physical information since, if two maxima are strong and are very close to each other, usually the LCS goes through both maxima and thus the distinction between them is no longer necessary. However, it is also possible that two close maxima may give rise to different LCS: in this situation we miss one LCS because we keep only one maximum. In the following we will illustrate in a specific case how the maximization distance can affect the resulting LCS and the physical information that we can obtain on the system.

In our simulations we performed a series of tests to tune the value of the maximization distance in order to find the optimal value that allows us to characterize the behavior of the system avoiding to have to deal with too many structures. We used a resolution of 600 points in the x -direction and the number of points in y -direction is set such as to have the same spatial resolution, i.e. $\Delta x = \Delta y$.

Another critical parameter is the interval $z - z_0$ chosen in the computation of the Cauchy-Green tensor. In fact, if this interval is too small, we risk selecting structures that last for a too short z -interval: for example, we could find LCS also in a non chaotic region, since two KAM tori with different velocities could be seen as divergent trajectories if the evolution time of the system is too small. On the other hand, if the integration interval is too long, the computational time grows and it may become very difficult to follow the eigenvectors of the Cauchy Green tensor. Moreover, as this interval increases, LCS tend to converge to the corresponding invariant manifolds which, as stated in Article *I*, are characterized by a very convoluted structure. Choosing carefully this parameter we are able to find structures with relatively simpler patterns which describe the coherent behavior of the system on a shorter interval. Finally, if the z interval is too long, the LCS technique itself could be wrong because the LCS are computed using linear techniques (see Eq.(5) of Article *I*). In order to avoid the problems related to a possible bad choice of the z interval, the Cauchy-Green tensor has been computed by taking, in the periodic case, the numerical value of $\nabla\phi_{z_0}^z(x_0, y_0)$ every $8L_z = 4 \cdot 32\pi$. This means that the FTLE field is calculated after every 4 z -loops and that we can take, among the points that are maxima of FTLE field at the end of z -interval, those points that have after each 4 z -loops a value of the FTLE larger than the FTLE mean value (computed with the values taken at the grid points). Since in our simulation the interval $z - z_0$ is 16 loops, this corresponds to three checks. With this check we ensure that we take as a starting point a point that repels particles at each time instant. In other words, we want to take a point that has

a good repulsion property during the 16 loops of the simulation interval, although this does not necessarily imply that the repulsion properties can be extended to longer integration intervals.

Finally, special attention has been paid to the problem of noise arising from the use of a finite grid. This problem is enhanced in a chaotic system and is mitigated here, as mentioned before, by avoiding spurious maxima present only at the end of the $z - z_0$ interval and by filtering the LCS by means of the criterion described above.

III. THE z -PERIODIC CASE

In this section we show the simulation results that we have obtained considering the Hamiltonian for the magnetic field line trajectories at a fixed physical time. We choose $t = 415$, i.e. before the onset of fully developed chaos.

A. Poincaré map

As stated above, once the physical time has been fixed we can exploit the periodicity of the system along the z -direction and apply the Poincaré map technique by plotting the magnetic line intersection points in the x - y plane after each periodicity interval in z starting from a given initial value of z that defines the section chosen. This kind of plot is very useful since it provides information on the topological aspect of the magnetic field configuration, identifying the regions where the trajectories are regular and those where they are chaotic. Although the Poincaré map is fundamental to study a time periodic dynamical system, the LCS technique allows a more refined analysis, as it makes it possible to further partition the regions characterized by a chaotic behavior into sub-regions where trajectories have a qualitatively different behavior on the time intervals which characterize the LCS. Here we focus on two sections, at $z = 0$, and $z = L_z/2$ respectively, and restrict the integration domain in the x -direction to the region in between the two initial resonant surfaces where chaos develops first i.e., to $0 < x < 0.8$ and $-2\pi < y < 2\pi$. The corresponding plot for $z = 0$ is shown in Fig.1. We note that a chaotic region exists between the two island chains that correspond to the initially imposed perturbations. However regular regions survive in the chaotic sea: in particular the regular region having $m = 3$ indicated in the figure splits the domain in two sub-domains.

B. Lagrangian coherent structures

To find the LCS it is first necessary to compute the field of the finite time Lyapunov exponents (see Secs. V and V B of Article *I*) and then proceed with the trajectory integration starting from the points with the largest

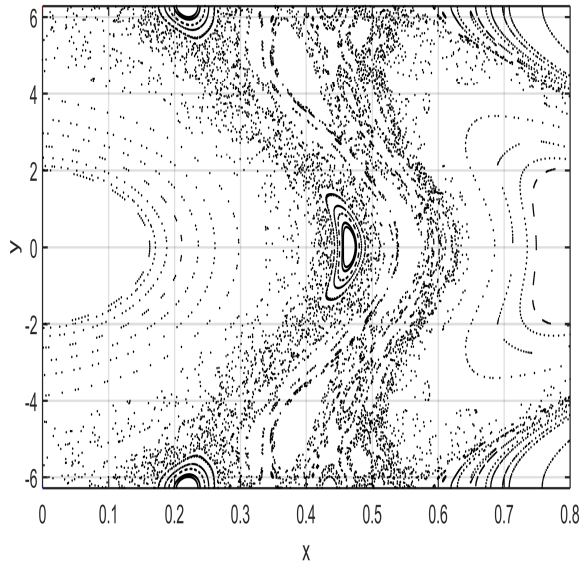


FIG. 1: Poincaré map at $z = 0$ of the magnetic configuration taken at $t = 415$. The map has been obtained evolving 150 initial conditions for $100L_z$. The initial conditions are uniformly distributed in the x -direction in the interval $[0, 0.8]$ and have $y = -2\pi$. The white regions correspond to trajectories (i.e. to magnetic field lines) on regular surfaces in the extended x, y, z phase space. The larger ones at the edge of the domain are the magnetic islands corresponding to the initial perturbations, while the regular region, that for $y = -2\pi$ is located approximately between $x = 0.35$ and $x = 0.4$, corresponds to a chain having $m = 3$ and splits the chaotic region in two sub-domains.

eigenvalue λ_{max} . The FTLE field is shown in Fig. 2. In the following we restrict our search to repelling LCS since we can exploit the space-time reflection symmetry $y \rightarrow -y, z \rightarrow -z$ introduced in Sec. VIA of Article I in order to find the attractive LCS which are thus obtained by mirror reflection of the repelling ones with respect to the $y = 0$ axis.

In Fig. 3 the LCS that we have identified with the numerical procedure described in Sec.IIB are overplotted on the Poincaré map. The repelling (attractive) structures are drawn in red (blue). We recall that in the small amplitude linear phase the two perturbations with different helicities evolve independently from each other and each of them induces a magnetic island chain around its resonant surface. If the Hamiltonian does not depend on z , these islands are delimited by the separatrices that are formed through the smooth connection of stable and unstable manifolds and that act as barriers. Here the smooth connection between stable and unstable manifolds is broken since the magnetic configuration does not correspond to an autonomous dynamical system. The footprint of the breaking can be recognized in Fig.3 close

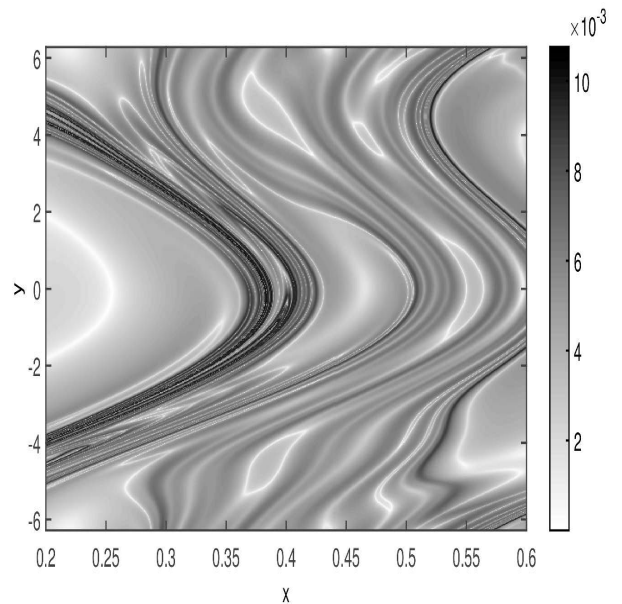


FIG. 2: FTLE field for the Hamiltonian at $t = 415$, on the plane $z = 0$. 500 points in x , and 7850 in y have been used so as to have the same resolution in both the directions. The darker shading corresponds to larger values of the eigenvalue λ_{max} of the Cauchy-Green tensor.

to the regular regions corresponding to the initial perturbations in the lobe-like shape that the LCS exhibit when approaching the edge of the domain. Since LCS mark the most repelling (attractive) material lines, they tend to follow the stable (unstable) manifolds that in non the autonomous case continue to intersect the unstable (stable) manifolds. In Fig.3 we mark with green arrows the most visible intersections that give rise to the lobes. In principle, the intersection should continue to generate a complex tangle but our numerical integration can not follow the manifold oscillations indefinitely.

In order to test the robustness of these LCS as barriers we performed a series of trajectory integration of magnetic field lines considering an initial set of 20 initial conditions at a given position and letting these trajectories evolve for $80L_z$. All the initial conditions (i.c.) are localized into a radius of 0.003. Then we plot their position in the $x-y$ phase space at every crossing of the the $z = 0$ section on which we have calculated the LCS. Figs. 4-6 confirm that the LCS that we have found act as strong barriers, since there is no flux through them on the considered time-span unless we consider regions with lobes and tangles. The location of the initial conditions is marked by an arrow in the figures. In the left panel of Fig.4, by taking the initial conditions very close to the KAM surfaces that are still present in the chaotic sea that forms between the two main magnetic islands, we see how the LCS confine the evolution of these trajectories. On the contrary, in the right panel of Fig.4 we

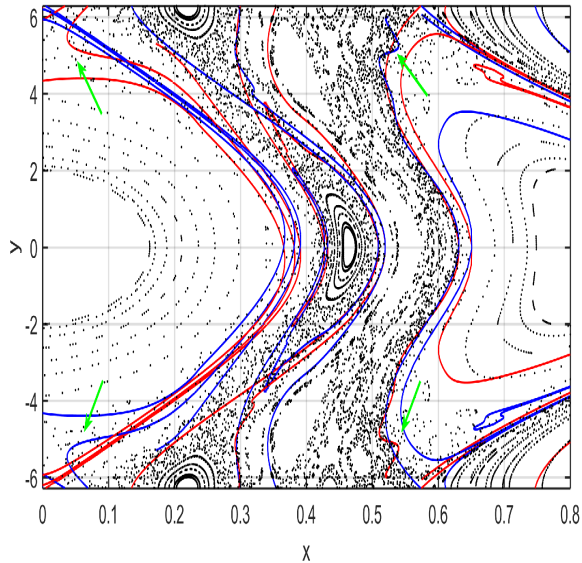


FIG. 3: Most important LCS overplotted on the Poincaré map at $z = 0$ and $t = 415$. The repelling (attractive) structures are drawn in red (blue). The green arrows indicate where the lobes and the tangle form.

set the initial conditions very close to a repelling LCS. In that region lobes and tangles are expected, although they are not visible due to the small resolution: with the adopted resolution we are able to follow the manifolds of the main islands, corresponding to the $m = 1$ mode but we cannot follow the manifolds of the smaller islands. In this region, according to the lobe dynamics briefly recalled in Sec. III of Article I, particles can cross the barriers. In the remaining Figs. 5,6 the role of different LCS is again tested using the same technique.

Examining the plots of the LCS shown in the figures we note that the repelling LCS, red lines in Fig.3 (and similarly the attractive LCS, blue lines) appear not to be periodic in the y direction. Actually this is a numerical effect related partly to the size of the integration grid and partly to the setting of the maximization distance described in Sec.II.B. In fact, decreasing the maximization distance used when selecting the FTLE maxima, additional LCS arise among which are those that match, at the edges of the y domain, the structures shown in the plots.

IV. THE z -NON PERIODIC CASE

In this section we consider the case of a magnetic field that evolves in physical time. This implies that a charged particle moving in the plasma sees a time varying magnetic field during its motion. The main questions that we intend to address are: how do the LCS change with

physical time, how different are the new LCS from those found at the fixed physical time $t = 415$ and finally if and how particles can cross LCS constructed for particles with a different velocity.

We examined a time interval extending over 10 normalized units from $t_1 = 415$ to $t_2 = 425$. Chaos has developed during this time interval as shown by the Poincaré map in Fig.7 for $t = 425$ i.e. at the end of the interval.

We adopt the simplified model, where particles move with a constant velocity V along the z -direction only, described in Sec. VIB of Article I. Then the new Hamiltonian is given by the modified flux function

$$\psi_V(x, y, z) \equiv \psi(x, y, z, t = (z - z_0)/V). \quad (4)$$

(see Eq.(21) of Article I) where the physical time dependence is chosen according to Eq.(3) and the dependence of ψ_V on the z variable combines the spatial and the time dependence of the magnetic configuration, as seen by a particle streaming with velocity V along a field line. We use this Hamiltonian to calculate LCS for different values of the velocity V . Note that, although simulations with different values of V have been performed, unless specified, the LCS shown in the figures are those for particles with velocity $V = 1000$. With this value the particles perform 10 z -loops in one time interval. This is a compromise between having a magnetic field that does not evolve too fast during the motion of particles and being able to show the dependence of the LCS on the velocity V and to investigate whether or not the LCS computed for a given velocity V act as barrier also for particles with different velocities. In the following we will focus on particles with a positive velocity. We stress that in this model the z periodic case corresponds to the assumption that the particles move with infinite speed and thus experience a fixed magnetic configuration.

First we note that if we keep the number of z -loops fixed the LCS that are found with increasing velocity turn out to be similar to those found in the periodic case, as expected when the particles travel time is much shorter than the time over which the magnetic field changes.

Thus, in order to show in a more evident way the LCS in a time evolving magnetic configuration as seen by a particle with velocity V , we integrate the Hamilton equations (2) with the flux function ψ_V in Eq.(4) over fixed time intervals i.e., in terms of the variable t instead of z using the relationship introduced below Eq. (21) of Article I, that is $t = (z - z_0)/V$. The change of variable from z to t and the definition of the time intervals need to be performed differently when computing repelling and when computing attractive LCS.

A. Repelling LCS

For the calculation of repelling LCS we relate t to z in the Hamilton equations such that $t - t_0 = (z - z_0)/V$

First we show how LCS evolve in time i.e. we calculate LCS at time $t = \bar{t}_0$ and position z_0 , then we "follow"

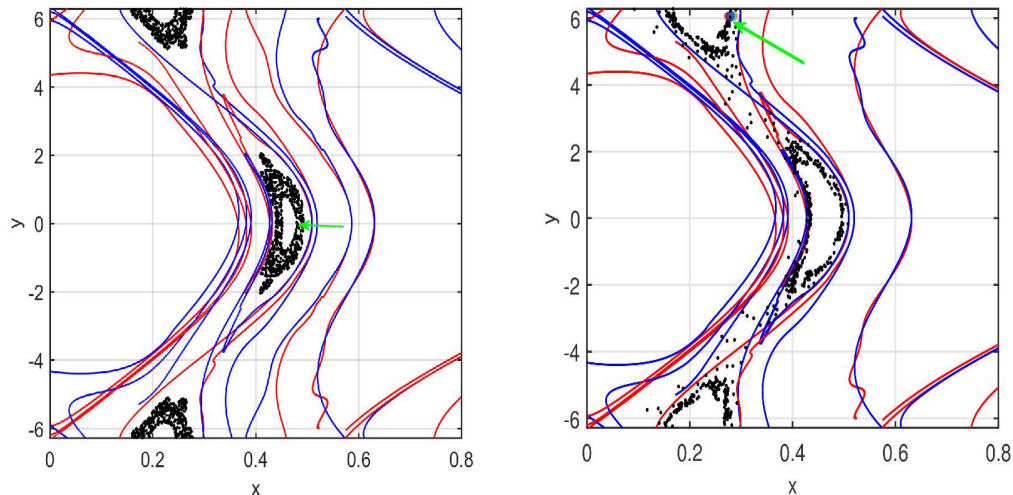


FIG. 4: LCS obtained using the Hamiltonian at $t = 415$. The left panel shows that the initial conditions taken in the regular region, bounded by hyperbolic LCS, remain confined inside this region. In the right panel the initial conditions are very close to a repelling LCS and, therefore, some particles escape according to the lobes dynamics. The location of the initial conditions is marked by an arrow.

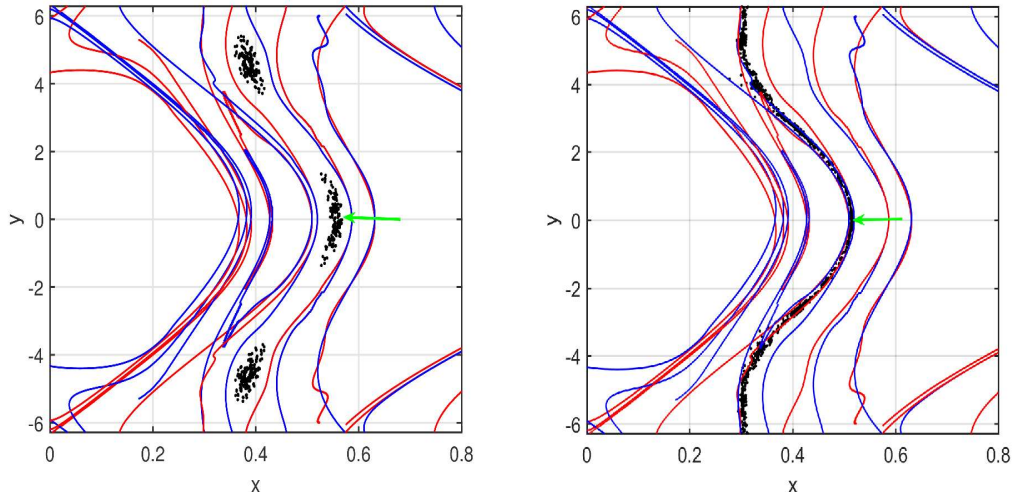


FIG. 5: LCS obtained for the Hamiltonian at $t = 415$. Both figures show how the drawn LCS act as barriers. Note that the marked trajectories belong to two different regions: in order to make the visualization easier in the right frame we have deleted the LCS that confine the set of initial conditions in the left frame. The location of the initial conditions is marked by an arrow.

the structures computing them at time \bar{t}_1 and position z_1 , at time \bar{t}_2 and position z_2 , and so on. To do this we set $V = 1000$ and choose the initial particle position, i.e. $z_0 = 0$, for all particles. Due to the long computational time and to the fact that the adopted method uses linear techniques, we choose to evaluate the LCS integrating the initial conditions for a maximum of 20 z -loops. For a velocity $V = 1000$, 20 z -loops correspond approximately to $\Delta t = 2$. In order to investigate how the time-dependent magnetic field can affect the evolution of the LCS, we evaluate the structures at different times

\bar{t}_n , starting from $\bar{t}_0 = 415$ since the time-independent analysis has been carried out at $t_1 = 415$. We divide the interval $[\bar{t}_0 = 415, \bar{t}_0 + \Delta t = 417]$ into sub-intervals of duration $\delta t = 0.1$. After each δt we calculate the LCS. Thus we obtain a set of LCS at the times $\bar{t}_n = 415, 415.1, 415.2$ up to 417. This allows us to determine how the LCS computed at $\bar{t}_0 = 415$ evolve in time.

Using these LCS data, we show how particles initially separated by a repelling LCS evolve in such a way that they remain apart and do not cross the LCS itself as it evolves in time.

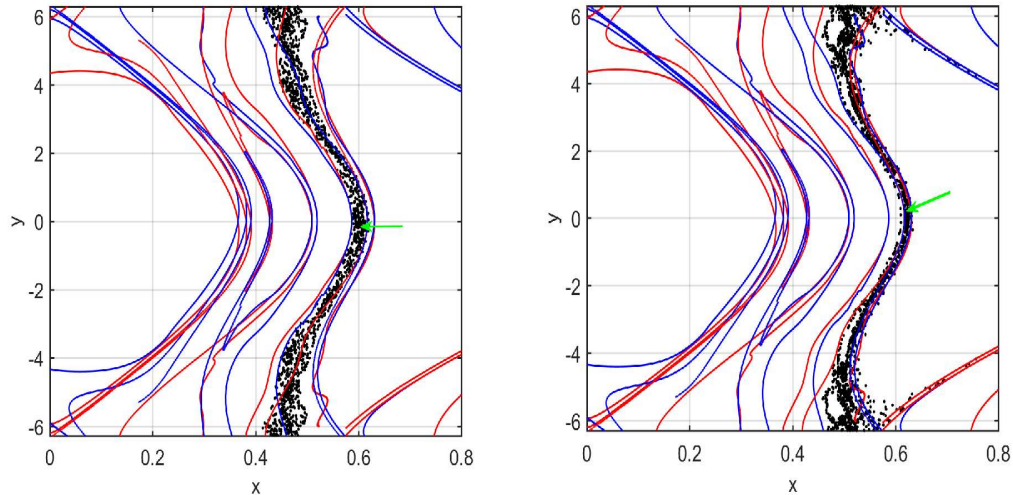


FIG. 6: LCS obtained using the Hamiltonian at $t = 415$. Both figures show how the drawn LCS act as barriers. Note that the figure in the right frame has been obtained reducing the value of the maximization distance with respect to that in the left frame. A new LCS arises and it splits the chaotic domain in the left frame in two sub-domains. Both domains are chaotic but they cannot communicate. This underlines the fact that if we take a smaller value of the maximization distance we can find additional transport barriers. The location of the initial conditions is marked by an arrow.

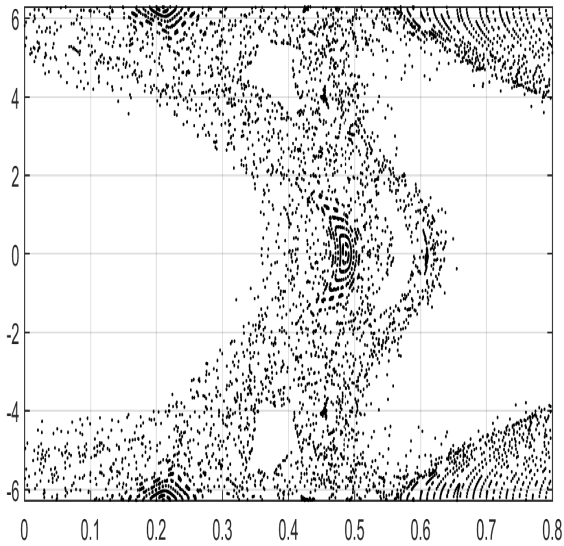


FIG. 7: Poincaré map at $z = 0$ and $t = 425$.

Particles with different velocities have different trajectories and, therefore, different LCS. We investigate the dependence of these structures with respect to V . As can be seen from the simulation results, LCS act locally, i.e. an exponential departure from a repelling LCS is not observed. Initial conditions feel the "repulsion" of a repelling LCS only when they are very close to it. Due to this local influence, two sets of i.c. divided by a repelling

LCS evolve initially in such a way as to maximize the distance from the repelling LCS, e.g. see Fig. (10). After this first stage they have different evolution.

B. Attractive LCS

For the attractive LCS we relate t to z in the Hamilton equations such that $t - t_{end} = (z - z_{end})/V$. As explained in Article 1 we compute the attractive LCS as repelling LCS of the backward time dynamics. We show how attractive structures affect particle dynamics and how essential they are in order to understand the transport features of the system. Looking only at the repelling LCS we can have only a partial understanding of the dynamics, e.g. we are able to say that two sets of i.c. divided from a repelling structure evolve in order to stay apart, but if we want to know also how "fast" are the mixing phenomena for those i.c., we need to calculate the attracting LCS. Following these considerations, we think that attractive LCS give a more intuitive description of the dynamics. They offer an intuitive understanding about how a big set of i.c. evolves. We remember that, when we evolve the system from $t_{end} = 417$ to $t_{end} - \Delta t = 415$ to compute the attracting LCS, the structures are those corresponding to $t_{end} = 417$ and they describe the behavior of particles at the time $t = 415$. Finally, we remark that also attractive LCS act as transport barriers. In the numerical results section, we exploit this fact to show that particles with velocity V_1 can cross barriers obtained considering a different velocity V_2 .

C. Numerical results

In Fig.8 two sets, each with 75 initial conditions, (marked green and black) are located on the two sides of a repelling LCS. The i.c. in each set are inside a circle with radius equal to 0.003. In Figs. 9-11 the evolution of these two sets is shown. During the first part of the evolution, Fig. 9, the particles move away from the nearby repelling LCS positioning themselves in such a way as to maximize their stretching in the perpendicular direction with respect to the LCS. In this phase the two set of i.c. behave similarly. In the left panel of Fig.10 it appears clearly that after only $\Delta t = 0.5$ the two sets of conditions have evolved obeying two different kinds of dynamics. Few time intervals are sufficient to recognize the chaotic dynamics of the black initial conditions: their distribution becomes more stretched and convoluted than that of the green conditions since they are influenced by the presence of a nearby attractive structure. This tendency is more and more evident with increasing time, as shown in Figs.10-11.

These results make the role of repelling and attractive LCS evident when describing the evolution of the system. In particular the presence of a nearby attractive LCS seems to give rise to faster mixing phenomena. In Figs.12 and 13 we show how particles feel the presence of attractive LCS. In Fig. 13 we use spatially localized initial conditions and show that these i.c. arrange themselves along the corresponding nearest attractive LCS. On the contrary, in Fig. 12 we use spatially spread initial conditions covering the region $x = [0.5, 0.6]$, $y = [0, -2]$.

There are 500 i.c. for each color: black particles in the region defined by $x = [0.5, 0.55]$ and $y = [0, -1]$; red particles in the region defined by $x = [0.5, 0.55]$ and $y = [-1, -2]$; green particles in the region defined by $x = [0.55, 0.6]$ and $y = [0, -1]$; brown particles in the region defined by $x = [0.55, 0.6]$ and $y = [-1, -2]$. The left panel shows the positions of the particles, starting at time $t = 416$, at the time $t = 418$. The blue lines are the attractive LCS computed starting from $t = 418$ to $t = 416$. The right panel shows the positions of particles, starting at time $t = 418$, at the time $t = 419$. The blue lines are the attractive LCS computed starting from $t = 419$ to $t = 418$.

The interesting behavior is that although the i.c. cover a wide region they evolve in such a way as to position themselves according to the attractive LCS. This is the reason why often LCS are referred to as the "skeleton" of the dynamics. This behavior is even more evident in the right panel of Fig. 12, where we present the results obtained for a shorter integration time interval ($\Delta t = 1$). In general, better results are obtained if shorter time intervals are used and this could be due to two reasons: the first one is linked to the fact that we use a linear approximation in deriving the Cauchy-Green tensor, and the second one is a consequence of the fact that when the time interval increases the structures become much more convoluted so that, in order to evaluate them in

a suitable way, it is necessary to have a higher spatial resolution.

Finally, we compare the LCS calculated for particles with $V = 1000$ with the dynamics of particles with different velocities. Taking the same initial conditions depicted in Fig. 13 but this time with $V = 200$, we find, as shown in Fig. 14, that they behave differently with respect to the LCS calculated for $V = 1000$. In the left panel of Fig. 14 we show the initial position of the particles and the repelling LCS computed integrating for $\Delta t = 10$ assuming $V = 200$ and, in the right panel, the new position of particles after $\Delta t = 10$ with the attracting LCS computed with $V = 1000$ (to show how particles with $V = 200$ can cross barriers obtained with velocity $V = 1000$) and $\Delta t = 2$. The choice $\Delta t = 10$ has been made in order to have the same number of z-loops (about 10) of the case $V = 1000$ shown in Fig. 13 and compare the results. While in Fig. 13 the particles arrange themselves along the attractive LCS, in Fig. 14 on the contrary such a relation between the attractive LCS (computed for particles with $V = 1000$) and the position of the particles (having $V = 200$) is not present. In particular, although the particle positions appear qualitatively similar to those in Fig. 13, black particles with $V = 200$ are shifted with respect to black particles having $V = 1000$. This is due to the fact that the magnetic field configuration at time $t = 425$ (see Poincaré plot in Fig. 7) has the $m = 2$ island chain shifted to the right with respect to its position at $t = 415$ (see Poincaré plot in Fig. 1). The same explanation also holds for some red particles that seem to be able to cross through a region that at time $t = 415$ is regular. Moreover, we can see also that red particles with $V = 200$ behave "more chaotically" than red particles in Fig. 13. This is probably due to the fact that, as can be seen in the left panel of Fig. 14, red i.c. are divided by two repelling LCS (red curves). Finally, also the magenta particles find themselves in a different region with respect to the case $V = 1000$ (although their behavior in the two cases is quite similar).

V. CONCLUSIONS

Lagrangian Coherent Structures have been shown to provide a very convenient tool in order to identify in a compact and easily visualizable way the main features of the dynamics of the physical system under consideration. Clearly, with large computers and long integration times one can recover all the needed information just following the individual trajectories of a large number of initial conditions. However LCS do not simply provide the salient features that can be extracted from such large scale integrations but provide a framework and a language to be used in characterizing the evolution of such features in time.

In this and in the accompanying paper (Article I) we have applied the LCS tool to the dynamics of charged particles in a magnetized plasma in the presence of a

time evolving reconnection instability. The LCS method is generally applicable without approximations by referring to the full particle dynamics in $3D$ coordinate space and by employing e.g., the exact particle Hamiltonian in time varying electromagnetic fields. Here, however, we have made use of two important simplifications with the aim of illustrating the method more than of obtaining exact results to be applied to a specific fusion experiment configuration. In the first model we have used the magnetic field lines in a slab configuration at a given physical instant of time as a proxy for the particle trajectories. In the second model we have introduced an elementary procedure in order to account in an approximate way for the fact that the magnetic configuration evolves in time during the particle motion. In both cases we have been confronted with a $2D$ phase space, much simpler than the full $6D$ phase space that would be required when solving the full particle dynamics. Clearly, this major simplification has been made possible by the fact that in the adopted configuration a strong and almost uniform magnetic field is present that, in a toroidal laboratory configuration, would correspond to the toroidal field. The first model has allowed us to relate the structures that govern the global dynamics of the particles to the evolution of the magnetic islands due to the development of magnetic reconnection. The second model has allowed us to show, even if in a rather schematic way, that these structures depend on the particle velocity (i.e. indirectly) on the particle energy. We conclude by reiterating that the methods developed in these two papers can be extended to more refined dynamical descriptions such as e.g. to a description based on the particle gyrokinetic approximation.

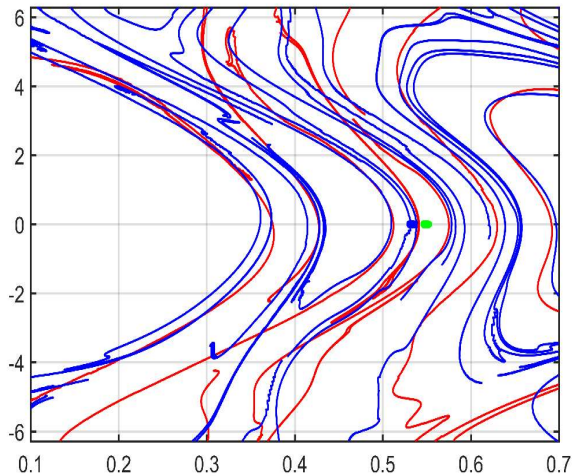


FIG. 8: Initial conditions split in two groups by a repelling LCS (red). Repelling LCS have been obtained with the system evolving from $t = 415$ to $t = 417$, and attracting LCS from $t = 417$ to $t = 415$.

ACKNOWLEDGMENTS

GDG and DG thank Dario Borgogno for fruitful discussions. Computational resources provided by hpc@polito, which is a project of Academic Computing within the Department of Control and Computer Engineering at the Politecnico di Torino (<http://www.hpc.polito.it>)

- ¹George Haller and Guocheng Yuan. Lagrangian coherent structures and mixing in two-dimensional turbulence. *Physica D: Nonlinear Phenomena*, 147(3):352–370, 2000.
- ²Dario Borgogno, Daniela Grasso, F Porcelli, F Califano, F Pegoraro, and D Farina. Aspects of three-dimensional magnetic reconnection. *Physics of plasmas*, 12(3):032309, 2005.
- ³Dario Borgogno, D Grasso, F Pegoraro, and TJ Schep. Stable and unstable invariant manifolds in a partially chaotic magnetic configuration generated by nonlinear reconnection. *Physics of Plasmas (1994-present)*, 15(10):102308, 2008.
- ⁴Dario Borgogno, Daniela Grasso, F Pegoraro, and TJ Schep. Barriers in the transition to global chaos in collisionless magnetic reconnection. i. ridges of the finite time lyapunov exponent field. *Physics of Plasmas (1994-present)*, 18(10):102307, 2011.
- ⁵K Onu, Florian Huhn, and George Haller. Lcs tool: A computational platform for lagrangian coherent structures. *Journal of Computational Science*, 7:26–36, 2015.

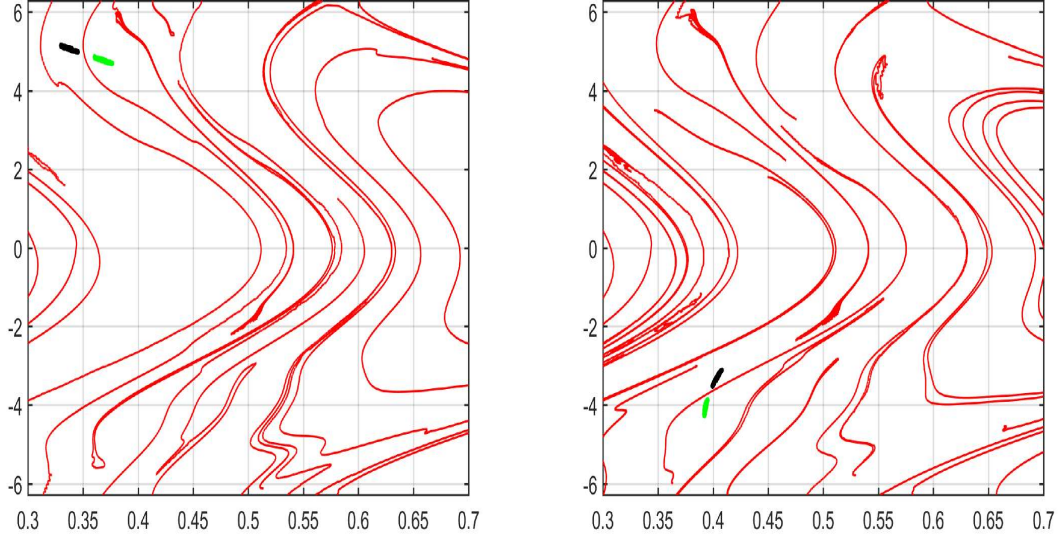


FIG. 9: Evolution of the initial conditions and of the LCS of Fig. 8 at $t = 415.1$ (left panel) and $t = 415.2$ (right panel). The LCS have been obtained with the system that evolves from $t = 415.1$ to $t = 417.1$ (left panel) and from $t = 415.2$ to $t = 417.2$ (right panel).

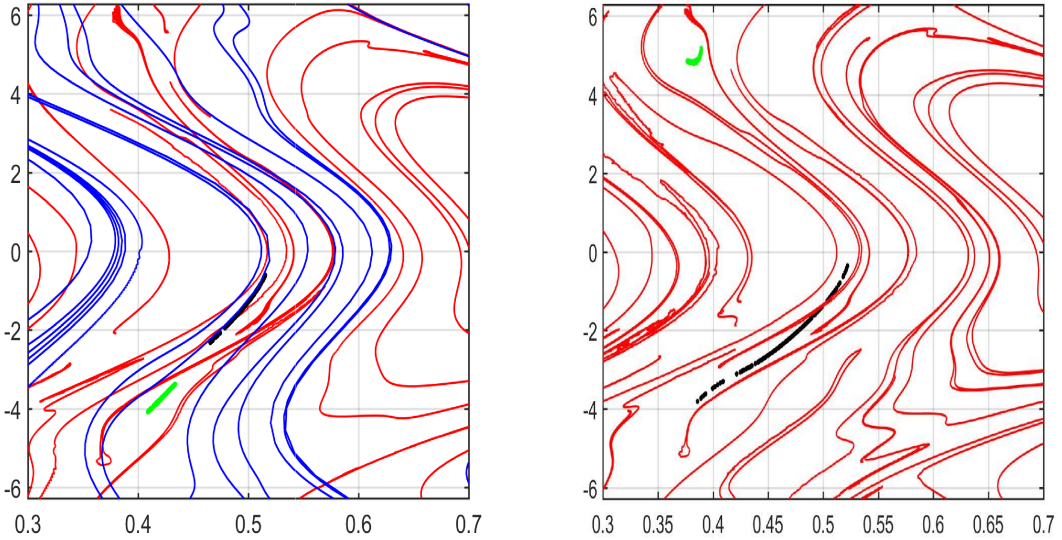


FIG. 10: Evolution of the initial conditions and of the repelling LCS (in red) of Fig. 8 at $t = 415.5$ (left panel) and $t = 416$ (right panel). The repelling LCS have been obtained with the system that evolves from $t = 415.5$ to $t = 417.5$ (left panel) and from $t = 416$ to $t = 418$ (right panel). In the left panel, the attracting LCS (blue curves) have been obtained with the system that evolves from $t = 415$ to $t = 415.5$. This is just to show how particles arrange themselves along attracting LCS computed for the same time interval of the particles evolution.

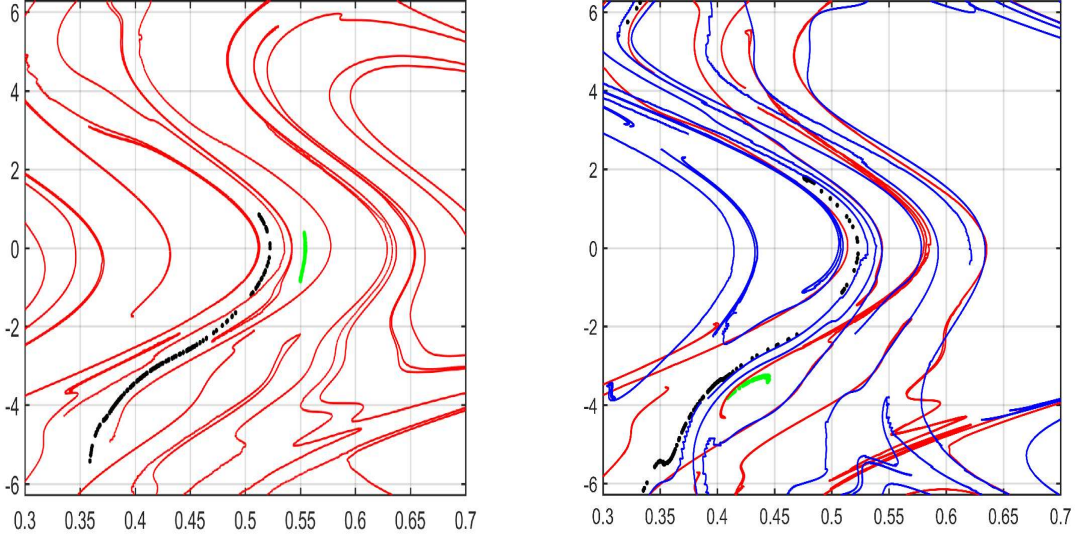


FIG. 11: Evolution of the initial conditions and of the repelling LCS of Fig. 8 at $t = 416.5$ (left panel) and $t = 417$ (right panel). The LCS have been obtained with the system that evolves from $t = 416.5$ to $t = 418.5$ (left panel) and from $t = 417$ to $t = 419$ (right panel). In the right panel, the attracting LCS (blue curves) have been obtained with the system that evolves from $t = 415$ to $t = 417$. This is just to show how particles arrange themselves along attracting LCS computed for the same time interval of the particles evolution.

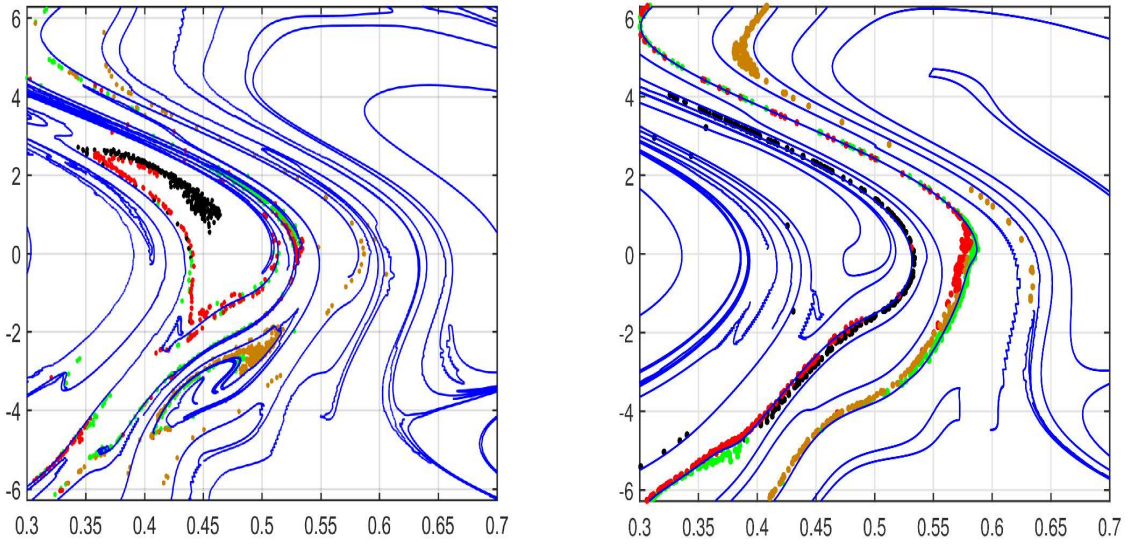


FIG. 12: Evolution of particles with $V = 1000$ according to the corresponding attractive LCS. For both figures the initial positions are the same: black particles $x = [0.5, 0.55], y = [0, -1]$, red $x = [0.5, 0.55], y = [-1, -2]$, green $x = [0.55, 0.6], y = [0, -1]$, brown $x = [0.55, 0.6], y = [-1, -2]$. There are 500 i.c. for each color. Particles in left panel start at time $t = 416$ and the figure shows their position at $t = 418$. Particles in the right panel start at $t = 418$ and in the plot their position at $t = 419$ is shown.

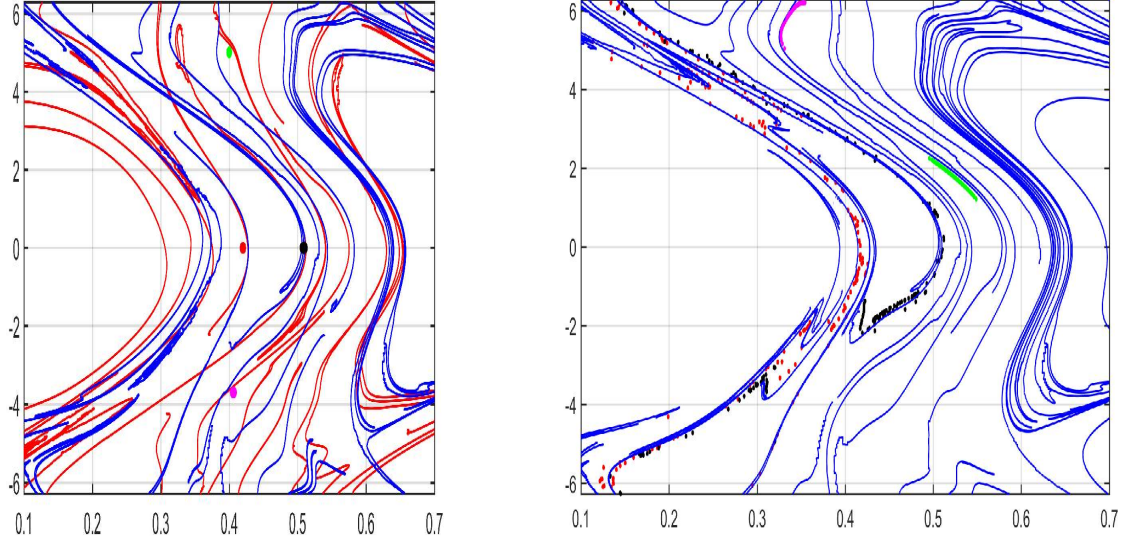


FIG. 13: Evolution of particles with $V = 1000$. On the left frame the initial conditions at time $t = 415$ are shown and on the right their evolution at time $t = 417$ is plotted. The aim of the picture is to underline how attractive LCS act as a skeleton for the dynamics. For clarity we only show attractive LCS (blue curves). Each color corresponds to 300 i.c.

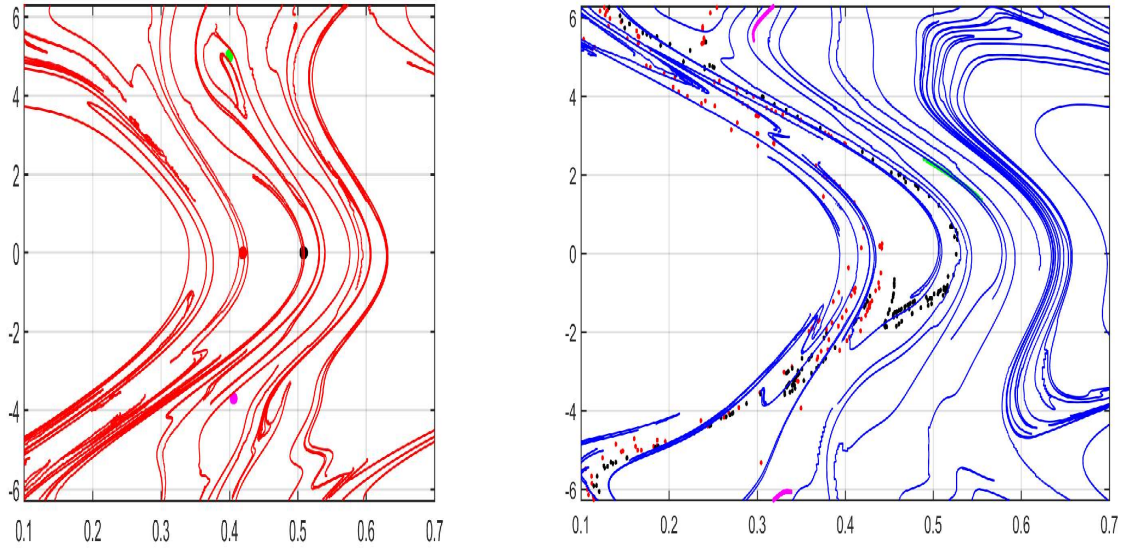


FIG. 14: Left panel: initial position at time $t = 415$ of particles and repelling LCS computed for particles with $V = 200$ with integration path $\Delta z = 19.9$ z-loops (corresponding to $\Delta t = 10$). Right panel: new position of particles having $V = 200$ at time $t = 425$ with attracting LCS computed for particles with $V = 1000$ with integration path $\Delta z = 19.9$ z-loops (corresponding to $\Delta t = 2$).